Minimal influence of reduced Arctic sea ice on coincident cold winters in mid-latitudes

Russell Blackport[1,*], James A. Screen[1], Karin van der Wiel[2] and Richard Bintanja[2,3]

[1]College of Engineering, Mathematics and Physical Sciences, University of Exeter, Exeter, UK

[2]Royal Netherlands Meteorological Institute, De Bilt, The Netherlands

[3]Energy and Sustainability Research Institute Groningen (ESRIG), Groningen University, Groningen, The Netherlands

*email: R.Blackport@exeter.ac.uk

Observations show that reduced regional sea ice cover is coincident with cold midlatitude winters on interannual timescales. However, it remains unclear if these observed links are causal and model experiments suggest they might not be. Here we apply two independent approaches to infer causality from, and to reconcile, observations and climate models. Models capture the observed correlations between reduced sea ice and cold midlatitude winters, but only when reduced sea ice coincides with anomalous heat transfer from the atmosphere to ocean, implying the atmosphere is driving the sea ice. Causal inference from the physics-based approach is corroborated by a lead-lag analysis, showing that circulation-driven temperature anomalies precede, but do not follow, reduced sea ice. Furthermore, no midlatitude cooling is found in modelling experiments with imposed future sea-ice loss. Our results robustly suggest that anomalous atmospheric circulation

simultaneously drives cold midlatitude winters and mild Arctic conditions, and reduced sea ice has a minimal influence on severe midlatitude winters.

Recent decades have seen rapid Arctic warming and sea-ice loss during winter[1–5]. At the same time, the midlatitude continents have experienced an increase in severe cold winters[3] in what is often referred to as the warm Arctic-cold continents pattern[6]. Similar links have also been found on interannual timescales[7,8]. Some studies have concluded that reduced sea ice or Arctic warming is a cause of cold midlatitude winters[7,8] and that, with continued Arctic sea-ice loss, this could lead to increased frequency of severe cold winters over the mid-latitudes, despite rising global temperatures.

To understand the mechanisms involved in connections between the Arctic and mid-latitudes, a common approach is to use correlation, regression or composite analysis to identify the atmospheric conditions coincident with reduced sea ice or warm Arctic temperatures, using observations or reanalyses[7–12]. In particular, one study suggested that wintertime warming in the East Siberian-Chukchi Sea generates a Rossby wave that causes cold Arctic air to flow into the mid-latitudes, causing severe winters over North America[7]. Similarly, wintertime warming in the Barents-Kara Sea was linked to cold winters over East Asia[7]. A follow-on study claimed that connections between warming in the East Siberian-Chukchi Sea and cooling over North America persisted into the spring, and lead to reduced terrestrial primary productivity and decreased crop-yields[11].

While this approach can identify connections between variables, it cannot, by itself, establish causality. To isolate the impacts of sea-ice loss, numerous modelling experiments have been performed in which atmospheric models are run with reduced sea ice cover. Many studies report no midlatitude cooling in response to the observed reduced sea ice and conclude that the severe winters can likely be attributed to internal atmospheric variability[13–17]. Others do detect an anticyclonic circulation and cooling response over Asia to sea ice reduction in the Barents-Kara Sea, but it is substantially weaker than what is inferred from analysis of observations[8,18,19]. One possible explanation for this apparent discrepancy between observational studies and modelling experiments is that models are unable to properly capture the response due to model deficiencies[19]. Alternatively, it is possible that the observed connections are not indicative of a causal response to reduced sea ice.

Here, we present evidence from observations and coupled climate model simulations that reduced sea ice and cold midlatitude continents are both simultaneously driven by the same large-scale atmospheric circulation patterns. The key advance in this study is to determine whether reduced winter Arctic sea ice is a cause of the cold midlatitude winters, through analysis of two independent and complementary methods to infer causality from interannual variability in observations and climate models. First, we use a novel, physically-motivated approach based on the direction of the surface turbulent (sensible + latent) heat flux (THF) over the Arctic regions; and second, we use lead-lag correlations. Furthermore, we also use model experiments with projected near-future sea ice loss imposed to examine if our conclusions based upon interannual variability also apply to multidecadal reductions in sea ice.

Using the turbulent heat flux to infer causality

Reductions in sea ice can cause an increase in upward THF at the surface, which warms and moistens the atmosphere[20,21]. This can potentially alter the large-scale atmospheric circulation through several mechanisms[3], leading to remote impacts far away from the Arctic. However, conversely, the large-scale circulation can drive changes in sea ice through thermodynamic and dynamical processes[22]. For example, warm and moist air can enter the Arctic and melt, or slow the growth, of sea ice through an increase in downwelling longwave radiation[22–25]. Critically, these warm intrusions are also associated with anomalous downward surface THF [23,24], hence the opposite of what is seen when the sea ice is driving the atmosphere. We argue therefore, that the sign of the surface THF anomaly provides physical insight into the predominant direction of ice-atmosphere interaction, with anomalous downward THF indicative of 'atmosphere driving ice'; or conversely, anomalous upward THF indicative of 'ice driving atmosphere'. A recent analysis used the THF to conclude that reduced Barents-Kara sea ice and cold winters in Asia were both driven by anomalous large-scale atmospheric circulation[26]; however, this study was hindered by the short observational record. Here we extend this analysis by using a novel approach to investigate cold winters over both Asia and North America and by using large ensembles (to ensure statistical robustness) of the current climate simulated by two climate models.

To separate the large-scale circulation patterns that are driving interannual variability in sea ice from those that are driven by sea ice variability, we use a simple method based on the sign of the THF anomaly over the Arctic region of interest to classify winters into two regimes. Winters when the atmosphere is primarily driven by sea ice are defined as those with a lower than average sea-ice area (SIA) and a positive THF anomaly (where positive is defined as from the

ocean to the atmosphere; Fig. 1c), or a higher than average SIA and a negative THF anomaly (Fig. 1a). Conversely, winters during which the atmosphere is driving the sea ice are defined as those with a lower than average SIA and a negative THF anomaly (Fig. 1d), or a higher than average SIA and a positive THF anomaly (Fig. 1b). After the classification of each winter we perform a linear regression of atmospheric fields onto the SIA separately for these two regimes to determine the large-scale circulation and temperature patterns associated with a reduction in sea ice, both when the ice is driving the atmosphere and when the atmosphere is driving the sea ice.

Interactions and feedbacks between sea ice and the atmosphere occur on a range of timescales, including shorter than a season. For example, it is hypothetically possible that within a season reduced sea ice (upward THF) could force an atmospheric circulation response that then induced further sea ice loss via a downward THF. Using the seasonal average THF for classification could yield misleading results if this were a common occurrence. To check if our approach is sensitive to the time averaging period, we also applied the THF classification to monthly averages. Importantly, we found our conclusions to be robust to the use of seasonal or monthly means. For brevity, we present the seasonal analysis in the main paper and provide the corroborating monthly analysis in the Supplementary Information. Further confirmation of the robustness of our conclusions is provided by complementary analyses using sub-seasonal lead-lag regressions. The lead-lag analysis provides an independent method to infer causality and does not rely on the THF, which may be unreliable in models or reanalysis[27].

Arctic links to cold North American winters

We first perform linear regressions of sea level pressure (SLP) and surface air temperature (SAT) onto the Chukchi-Bering Sea (CBS; 165°E-155°W, 55°-70°N) sea-ice area index for all winters, in the ERA-Interim[28] reanalysis and in large ensembles of simulations of the present-day climate from two state-of-the-art coupled ocean-atmosphere climate models (HadGEM2[29] and EC-Earth[30]). In ERA-Interim and the two models, reduced sea ice is associated with strong warming over the CBS region, cooling over North America, a cyclonic SLP anomaly to the west of the CBS region, and an anticyclonic anomaly to the east of the CBS region (Fig 2a-c). As identified by Ref 7, this SLP pattern will cause anomalous cold air advection into North America from the Arctic, resulting in colder than normal winters. However, it is also associated with the advection of warm, moist air from the south into the CBS region, which questions whether the reduced sea ice is driving the circulation anomaly, or instead, whether the circulation is driving both the reduced sea ice conditions and cold temperatures over North America. The robustness of the large-scale circulation and temperature patterns associated with sea ice variability between the two models used here is in agreement with Ref 7, in which it was found that all models participating in the Coupled Model Intercomparison Project 5 (CMIP5) exhibit a negative regression coefficient between the East Siberian-Chukchi Sea and North American SAT during winter.

It is clear from Fig. 2a-c that the Arctic is strongly linked with cold North American winters, however this does not mean that the relationship is causal. Figure 2d-f shows the SLP and SAT regressed onto the CBS sea ice index during winters when sea ice is driving the atmosphere. In ERA-Interim and in both models, there is an absence of cooling over North America when the sea ice is driving the atmosphere, despite warming over the CBS region. The SLP pattern is also

consistent between ERA-Interim and the models, with an anomalous cyclonic anomaly near and to the south of the CBS region (i.e., a deepening of the Aleutian Low). This is a common response to reduced sea ice seen in modelling experiments[31–37]. In contrast, during winters when the atmosphere is driving the sea ice (Fig. 2g-i), reduced sea ice is associated with strong cooling over North America and a SLP anomaly pattern that strongly resembles that shown in Fig. 2a-c (with SLP pattern correlations of 0.93, 0.82 and 0.94 in ERA-Interim, HadGEM2 and EC-Earth). As mentioned earlier, similar results are found in each individual month during winter (Supplementary Fig. 1 and 2 and Supplementary Discussion 1) confirming the results are not sensitive to the time averaging period, and are consistent throughout the winter months. These results suggest that reduced sea ice has a weak influence on cold winters over North America, but instead the anomalous large-scale circulation simultaneously causes reduced CBS sea ice, Arctic warming and cold North American winters. We also reach the same conclusions during springtime, when Arctic warming has been linked to reduced primary productivity over North America through the same circulation patterns[11] (Supplementary Fig. 3 and Supplementary Discussion 2).

While the above analysis suggests reductions in sea ice are not the main cause of midlatitude cooling, it does not rule out the possibility that, within the timeframe analysed (a season), reduced sea ice could cause the anticyclonic circulation anomaly, leading to warm air advection and a downward THF anomaly over the CBS region. We can confidently rule out this possibility however, based on lead-lag regressions on sub-seasonal timescales. One month ahead of reduced sea ice, there is downward THF anomaly in the CBS region (Supplementary Fig. 4), strong cooling over North America (Fig. 3a-c) and the SLP and SAT patterns strongly resemble those

found during winters when the atmosphere is driving the sea ice. In contrast, one month after the reduced sea ice, despite the persistence of the reduced sea ice and a strong upward THF anomaly (Supplementary Fig. 4), there is very little cooling found over North America and no downstream anticyclonic anomaly in either of the models or ERA-Interim (Fig 3g-i). In the models, there is a low-pressure anomaly over the CBS region that strongly resemble the patterns found during winters when the ice is driving the atmosphere. Again, similar results are found for each individual winter month in the models (Supplementary Fig. 5 and 6). Furthermore, we find similar lead-lag relationships based on sub-monthly data (Supplementary Fig. 7 and Supplementary Discussion 1). The fact that two methodologies – one based on the sign of the heat flux and the other based on time leads and lags – produce the same results provides strong evidence that reduced sea ice is not the main cause of severe midlatitude winters. Lastly, we consider the possibility of a lagged winter cooling response to autumn sea-ice loss, as proposed by past work[8,18] albeit in the context of Eurasian cooling rather than North American cooling. We find no evidence to support such a connection between autumn sea ice and the winter atmospheric circulation or North American temperatures (Supplementary Fig 8 and Supplementary Discussion 3). Thus, we conclude that neither reduced autumn or winter sea ice is a likely a major cause of cold North American winters.

Arctic links to cold Asian winters

We now turn to the abnormally cold Asian winters, which are associated with reduced sea ice in the Barents-Kara Sea (BKS; 30°-70°E, 70°-80°N). This connection has received more attention than that between CBS sea ice and North American winters, but there is no consensus on the causal role of sea ice in driving cold Asian winters[8,13–15,18,38]. Regressions of SAT and SLP onto

the BKS sea-ice area index confirm that reduced sea ice is coincident with cold winters over Asia (Fig. 4a-c). The SLP pattern associated with reduced BKS ice consists of an anomalous anticyclonic anomaly over Northern Russia and an anomalous cyclonic anomaly over the North Pole. Similar to the circulation anomalies associated with reduced CBS ice, this SLP pattern causes cold air advection into Asia, but it is also associated with the advection of warm and moist air into the BKS region from the North Atlantic[25,39,40]. We note that the magnitudes of the SLP and SAT regressions appear to be weaker in the models than in the reanalysis. However, they are within the distribution of possible values obtained from 38-year samples of model output (Supplementary Fig. 9 and Supplementary Discussion 4), suggesting the larger magnitude regressions in the reanalysis could be a result of sampling uncertainty (i.e., internal climate variability).

The midlatitude cooling and anomalous atmospheric circulation associated with reduced sea ice in the BKS region is only evident during winters when the atmosphere is driving the sea ice (Fig. 4g-i). In winters when the sea ice is driving the atmosphere (Fig. 4d-f), the models show only a weak low-pressure response over the regions of reduced sea ice and no cooling over Asia. In ERA-Interim, there is a small region of significant cooling in East Asia associated with a weak and not statistically significant high-pressure anomaly over Siberia. Though not seen in the models analysed here, this is consistent with some modelling experiments that suggest a weak East Asian cooling in response to sea-ice loss[8,18,31,35,41]. Nevertheless, even in ERA-Interim, regression coefficients between BKS sea ice and Asian SAT are more than 4 times larger in winters when the atmosphere is driving ice compared to when the ice is driving the atmosphere. Thus, reduced BKS sea ice does not appear to be the dominant cause of the coincident Asian

cooling, and the reanalysis record is too short to be conclusive. Sub-seasonal lead-lag regressions with BKS sea ice further suggest that sea ice is not driving the cooling, since cooling is present one month prior, but not one month following, reduced sea ice (Supplementary Fig. 10 and Supplementary Discussion 5). Here we have focused on the relationship with winter sea ice; however, it is also been suggested that autumn sea ice in the BKS may influence winter midlatitude temperatures over Asia[8,18]. Indeed, consistent with past papers we find a statistically significant correlation in ERA-Interim (but not in the models) between September or October BKS ice and winter Asian temperature (Supplementary Fig. 8 and Supplementary Discussion 3). This apparent connection does not occur via the winter circulation anomalies identified in Fig. 4a and might occur via a stratospheric pathway[42–45], but again, the reanalysis record is too short to be conclusive. Also, there is evidence that this association may be largely driven by atmospheric circulation variability and not sea ice[46].

Response to near-future sea-ice loss

Our results so far strongly suggest that reduced sea ice is not the predominant cause of cold midlatitude winters on interannual time-scales. This implies that ongoing sea-ice loss would not be expected to lead to winter cooling in the future, assuming that similar processes control the atmospheric response to interannual and multidecadal reductions in sea ice. To explicitly test this, we turn to coupled ocean-atmosphere experiments (from the HadGEM2 model) in which sea-ice loss has been imposed in isolation, without any change in external forcing such as greenhouse gases. More specifically, the sea ice extent is constrained to be approximately equal to that projected at 2 °C global warming above pre-industrial levels. We find that the same correlation between winter sea ice, the atmospheric circulation and midlatitude temperatures seen

in the present-day climate is also present in our simulation with diminished sea ice (Supplementary Fig 11 and 12). Despite this, and even though there is less sea ice in the CBS and BKS regions in the future compared to now (Fig 5a), we find no appreciable differences in midlatitude temperatures (Fig 5b). The lack of cooling in response to future sea-ice loss is entirely consistent with our interpretation of the interannual variability: that variations in sea ice are not a major driver of midlatitude temperature. The SLP response to future sea-ice loss is dominated by a shift towards the negative phase of the North Atlantic Oscillation (NAO), which may be expected to lead to cooling over Europe; however this is absent, likely a result of the thermodynamical warming response offsetting the dynamical cooling response[47].

Reconciling models and observations

Our results help reconcile modelling studies, which generally find no or weak midlatitude cooling in response to sea-ice loss, and observational based studies, which have inferred a larger cooling response to sea-ice loss. We have shown that cold midlatitude winters are coincident with reduced sea ice in observations and in two climate models, suggesting models are capable of capturing the relevant processes. Thus, model biases do not appear to be the root cause of the apparent divergence between modelling and observational studies. Instead, we argue this discrepancy arises due to the (mis)interpretation of causality. We cannot fully rule out that model biases may also contribute, but they do not appear necessary to explain the discrepancy between model- and observation-based studies.

We have presented evidence from three lines of enquiry - the direction of the THF, lead-lag regressions and model experiments with future sea-ice loss imposed – that strongly suggests that

reduced sea ice has a minimal, if any, influence on cold midlatitude winters. We find some evidence that reduced sea ice may contribute to cold winters in East Asia, but the influence of sea ice appears very weak compared to internal variability, and is insufficient to explain the observed correlation between reduced sea ice and cold winters. We conclude that covariability between Arctic and midlatitude temperatures manifests because of large-scale atmospheric circulation anomalies that are predominantly a cause of, and not a response to, variations in sea ice. Therefore, we surmise that it is unlikely that cold winters and associated impacts over the mid-latitudes will increase in frequency as a result of continued winter Arctic sea ice loss.

Correspondence and requests for materials should be addressed to R. Bl.

Acknowledgments

We thank the ECMWF for making the ERA-Interim reanalysis data available for use. The HadGEM2 model simulations were performed on the ARCHER UK national computing service. R.Bl. and J.A.S were supported by Natural Environment Research Council grant NE/P006760/1.

Author contributions

R.Bl. conceived of the study, analysed the data and wrote the manuscript. J.A.S provided guidance writing the manuscript and interpreting the results. R.Bl. and K.W. performed the climate model simulations. All authors contributed to the design of model simulations and commented on the manuscript.

Competing interests

The authors declare no competing interests.

References

1. Screen, J. A. & Simmonds, I. The central role of diminishing sea ice in recent Arctic temperature amplification. *Nature* **464**, 1334–1337 (2010).
2. Walsh, J. E. Intensified warming of the Arctic: Causes and impacts on middle latitudes. *Glob. Planet. Change* **117**, 52–63 (2014).
3. Cohen, J. *et al.* Recent Arctic amplification and extreme mid-latitude weather. *Nat. Geosci.* **7**, 627–637 (2014).
4. Stroeve, J., Holland, M. M., Meier, W., Scambos, T. & Serreze, M. Arctic sea ice decline: Faster than forecast. *Geophys. Res. Lett.* **34**, L09501 (2007).
5. Stroeve, J. C. *et al.* Trends in Arctic sea ice extent from CMIP5, CMIP3 and observations. *Geophys. Res. Lett.* **39**, L16502 (2012).
6. Overland, J. E., Wood, K. R. & Wang, M. Warm Arctic-cold continents: climate impacts of the newly open Arctic Sea. *Polar Res.* **30**, 15787 (2011).
7. Kug, J.-S. *et al.* Two distinct influences of Arctic warming on cold winters over North America and East Asia. *Nat. Geosci.* **8**, 759–762 (2015).
8. Mori, M., Watanabe, M., Shiogama, H., Inoue, J. & Kimoto, M. Robust Arctic sea-ice influence on the frequent Eurasian cold winters in past decades. *Nat. Geosci.* **7**, 869–873 (2014).
9. Inoue, J., Hori, M. E. & Takaya, K. The Role of Barents Sea Ice in the Wintertime Cyclone Track and Emergence of a Warm-Arctic Cold-Siberian Anomaly. *J. Clim.* **25**, 2561–2568 (2012).
10. Tang, Q., Zhang, X., Yang, X. & Francis, J. A. Cold winter extremes in northern continents linked to Arctic sea ice loss. *Environ. Res. Lett.* **8**, 014036 (2013).

11. Kim, J.-S. *et al.* Reduced North American terrestrial primary productivity linked to anomalous Arctic warming. *Nat. Geosci.* **10**, 572–576 (2017).
12. Cohen, J., Pfeiffer, K. & Francis, J. A. Warm Arctic episodes linked with increased frequency of extreme winter weather in the United States. *Nat. Commun.* **9**, 869 (2018).
13. McCusker, K. E., Fyfe, J. C. & Sigmond, M. Twenty-five winters of unexpected Eurasian cooling unlikely due to Arctic sea-ice loss. *Nat. Geosci.* **9**, 838–842 (2016).
14. Sun, L., Perlwitz, J. & Hoerling, M. What caused the recent "Warm Arctic, Cold Continents" trend pattern in winter temperatures? *Geophys. Res. Lett.* **43**, 5345–5352 (2016).
15. Collow, T. W., Wang, W. & Kumar, A. Simulations of Eurasian winter temperature trends in coupled and uncoupled CFSv2. *Adv. Atmospheric Sci.* **35**, 14–26 (2018).
16. Ogawa, F. *et al.* Evaluating Impacts of Recent Arctic Sea Ice Loss on the Northern Hemisphere Winter Climate Change. *Geophys. Res. Lett.* **45**, 3255–3263 (2018).
17. Koenigk, T. *et al.* Impact of Arctic sea ice variations on winter temperature anomalies in northern hemispheric land areas. *Clim. Dyn.* **52**, 3111–3137 (2019).
18. Honda, M., Inoue, J. & Yamane, S. Influence of low Arctic sea-ice minima on anomalously cold Eurasian winters. *Geophys. Res. Lett.* **36**, (2009).
19. Mori, M., Kosaka, Y., Watanabe, M., Nakamura, H. & Kimoto, M. A reconciled estimate of the influence of Arctic sea-ice loss on recent Eurasian cooling. *Nat. Clim. Change* **9**, 123 (2019).
20. Deser, C., Walsh, J. E. & Timlin, M. S. Arctic sea ice variability in the context of recent atmospheric circulation trends. *J. Clim.* **13**, 617–633 (2000).

21. Deser, C., Tomas, R., Alexander, M. & Lawrence, D. The Seasonal Atmospheric Response to Projected Arctic Sea Ice Loss in the Late Twenty-First Century. *J. Clim.* **23**, 333–351 (2010).
22. Park, H.-S., Lee, S., Son, S.-W., Feldstein, S. B. & Kosaka, Y. The Impact of Poleward Moisture and Sensible Heat Flux on Arctic Winter Sea Ice Variability. *J. Clim.* **28**, 5030–5040 (2015).
23. Woods, C. & Caballero, R. The Role of Moist Intrusions in Winter Arctic Warming and Sea Ice Decline. *J. Clim.* **29**, 4473–4485 (2016).
24. Lee, S., Gong, T., Feldstein, S. B., Screen, J. A. & Simmonds, I. Revisiting the Cause of the 1989–2009 Arctic Surface Warming Using the Surface Energy Budget: Downward Infrared Radiation Dominates the Surface Fluxes. *Geophys. Res. Lett.* **44**, 10,654-10,661 (2017).
25. Luo, B., Luo, D., Wu, L., Zhong, L. & Simmonds, I. Atmospheric circulation patterns which promote winter Arctic sea ice decline. *Environ. Res. Lett.* **12**, 054017 (2017).
26. Sorokina, S. A., Li, C., Wettstein, J. J. & Kvamstø, N. G. Observed Atmospheric Coupling between Barents Sea Ice and the Warm-Arctic Cold-Siberian Anomaly Pattern. *J. Clim.* **29**, 495–511 (2016).
27. Jakobson, E. *et al.* Validation of atmospheric reanalyses over the central Arctic Ocean. *Geophys. Res. Lett.* **39**, (2012).
28. Dee, D. P. *et al.* The ERA-Interim reanalysis: configuration and performance of the data assimilation system. *Q. J. R. Meteorol. Soc.* **137**, 553–597 (2011).
29. Martin, G. M. *et al.* The HadGEM2 family of Met Office Unified Model climate configurations. *Geosci Model Dev* **4**, 723–757 (2011).

30. Hazeleger, W. *et al.* EC-Earth V2.2: description and validation of a new seamless earth system prediction model. *Clim. Dyn.* **39**, 2611–2629 (2012).
31. Blackport, R. & Kushner, P. J. Isolating the Atmospheric Circulation Response to Arctic Sea Ice Loss in the Coupled Climate System. *J. Clim.* **30**, 2163–2185 (2017).
32. Blackport, R. & Kushner, P. J. The Transient and Equilibrium Climate Response to Rapid Summertime Sea Ice Loss in CCSM4. *J. Clim.* **29**, 401–417 (2016).
33. McCusker, K. E. *et al.* Remarkable separability of circulation response to Arctic sea ice loss and greenhouse gas forcing. *Geophys. Res. Lett.* **44**, 7955–7964 (2017).
34. Oudar, T. *et al.* Respective roles of direct GHG radiative forcing and induced Arctic sea ice loss on the Northern Hemisphere atmospheric circulation. *Clim. Dyn.* **49**, 3693–3713 (2017).
35. Peings, Y. & Magnusdottir, G. Response of the Wintertime Northern Hemisphere Atmospheric Circulation to Current and Projected Arctic Sea Ice Decline: A Numerical Study with CAM5. *J. Clim.* **27**, 244–264 (2014).
36. Deser, C., Sun, L., Tomas, R. A. & Screen, J. Does ocean coupling matter for the northern extratropical response to projected Arctic sea ice loss? *Geophys. Res. Lett.* **43**, 2149–2157 (2016).
37. Screen, J. A. *et al.* Consistency and discrepancy in the atmospheric response to Arctic sea-ice loss across climate models. *Nat. Geosci.* **11**, 155–163 (2018).
38. Screen, J. A. Simulated Atmospheric Response to Regional and Pan-Arctic Sea Ice Loss. *J. Clim.* **30**, 3945–3962 (2017).
39. Woods, C., Caballero, R. & Svensson, G. Large-scale circulation associated with moisture intrusions into the Arctic during winter. *Geophys. Res. Lett.* **40**, 4717–4721 (2013).

40. Sato, K., Inoue, J. & Watanabe, M. Influence of the Gulf Stream on the Barents Sea ice retreat and Eurasian coldness during early winter. *Environ. Res. Lett.* **9**, 084009 (2014).
41. Sun, L., Deser, C. & Tomas, R. A. Mechanisms of Stratospheric and Tropospheric Circulation Response to Projected Arctic Sea Ice Loss. *J. Clim.* **28**, 7824–7845 (2015).
42. Kim, B.-M. *et al.* Weakening of the stratospheric polar vortex by Arctic sea-ice loss. *Nat. Commun.* **5**, 4646 (2014).
43. Zhang, P., Wu, Y. & Smith, K. L. Prolonged effect of the stratospheric pathway in linking Barents–Kara Sea sea ice variability to the midlatitude circulation in a simplified model. *Clim. Dyn.* **50**, 527–539 (2018).
44. Nakamura, T. *et al.* The stratospheric pathway for Arctic impacts on midlatitude climate. *Geophys. Res. Lett.* **43**, 3494–3501 (2016).
45. Zhang, P. *et al.* A stratospheric pathway linking a colder Siberia to Barents-Kara Sea sea ice loss. *Sci. Adv.* **4**, eaat6025 (2018).
46. Peings, Y. Ural Blocking as a Driver of Early-Winter Stratospheric Warmings. *Geophys. Res. Lett.* **46**, (2019).
47. Screen, J. A. The missing Northern European winter cooling response to Arctic sea ice loss. *Nat. Commun.* **8**, 14603 (2017).

Methods

Models. We use two coupled ocean-atmosphere climate models: HadGEM2-ES and EC-Earth V2.3. Both are the versions used in the Coupled Model Intercomparison Project 5 (CMIP5). The atmospheric model for HadGEM2-ES is the Met Office Unified Model version 6.6.3 run at N96

horizontal resolution (1.875 °longitude x 1.25° latitude) and 38 vertical levels. The ocean model used is NEMO run at approximately 1° resolution (increasing to 1/3° at the equator) and 40 vertical levels. The atmospheric model in EC-Earth V2.3 is the Integrated Forecasting System (IFS) cycle 31r1 run at 1.125° resolution and 62 vertical layers and the ocean model is NEMO with 1° resolution (increasing to 1/3° at the equator) and 42 vertical layers.

Model simulations. For each model, a present-day ensemble consisting of 400 realisations of 5 years in length were performed for a total of 2000 years (with only 1600 full winters as the runs started on January 1st). The simulations were forced with the RCP8.5 emissions scenario for the years 2008-2012 for HadGEM2 and 2035-2039 from EC-Earth. These time periods correspond to when the absolute global mean surface temperature (GMST) from the ensemble mean of the available CMIP5 RCP8.5 simulations matched the observed absolute GMST for the period 2011-2015 from HadCRUT4 observations. Initial conditions for the 400 realizations were generated by making 25 atmospheric perturbations branched off from 16 different climate states from the available RCP8.5 simulations. For HadGEM2 there were only 4 available RCP8.5 realizations, so 3 additional simulations were branched off each existing run at the year 1990 in the historical CMIP5 simulations and then forced with historical and RCP8.5 forcing until 2008, to generate the 16 initial climate states.

The reduced sea ice simulations using HadGEM2 were identical to the present-day ensemble described above except two sea-ice albedo parameters were modified to reduce the sea ice to approximately match the sea-ice extent at 2°C global warming above pre-industrial levels. We decreased the albedo of the cold deep snow on top of the sea ice from 0.80 to 0.05 and increased

409 the albedo of snow-free sea ice from 0.61 to 0.66. The large decrease in albedo of cold deep
410 snow on top of the sea ice results in more sunlight absorbed by the sea ice, leading to year-round
411 sea ice melt, but with larger reductions in summer and autumn relative to winter. The small
412 increase in snow-free albedo acts to increase summer and autumn sea ice while having little
413 impact on winter, resulting in a more realistic seasonal cycle of sea ice loss. The response shown
414 in Fig. 5 is calculated by subtracting the mean over all 1600 full winters from the reduced sea ice
415 simulations from the mean of the 1600 full winters from the present-day simulations.
416
417 **Regression analysis.** We linearly regress the winter (December-February) average SAT and SLP
418 fields onto standardised sea-ice area indices for ERA-Interim and each model. All 1600 full
419 winters for each model, and 38 years (1979/80-2016/17) for ERA-Interim were used. Sea ice
420 indices were created by calculating the sea-ice area (area of grid cells weighted by sea ice
421 concentration) over the CBS region (165°E-155°W, 55°-70°N) and BKS region (30°-70°E, 70°-
422 80°N) and averaging over the winter season. The sea-ice area time series were then divided by
423 the standard deviation and the sign was reversed, so that regression maps represent the field
424 associated with a one standard deviation reduction in sea-ice area. The standard deviation of the
425 sea-ice area are 0.15, 0.14 and 0.13 million km^2 for ERA-Interim, HadGEM2 and EC-Earth
426 respectively for the CBS region, and 0.15, 0.15 and 0.14 million km^2 for the BKS region. All
427 ERA-Interim data were linearly detrended after seasonal averaging was performed. For the
428 regressions performed on the two regimes in Fig. 2d-i and Fig. 4d-i, the sea ice index is not re-
429 standardised after classifying, so that the fields represent the associations with the same sea ice
430 anomaly regardless of whether it is the ice driving the atmosphere or atmosphere driving the ice.
431

The CBS region that we used is shifted further south compared to the region used by Ref 7 to capture the region with the largest sea ice variability. Our analysis and conclusions are not sensitive to small changes to the regional definitions or whether passive microwave data from the National Snow and Ice Data Center (NSIDC)[48] was used to calculate sea ice indices instead of ERA-Interim (the correlation between ERA-Interim and NSIDC sea ice indices is 0.98 for both regions). We also come to the same conclusions if Arctic SAT is used instead of sea ice area as there is a strong correlation between two variables in DJF means ($r = -0.89$ for both regions in ERA-Interim). Our results are also not sensitive to small changes (+/- 0.5 standard deviations) in the THF threshold used to classify each year as 'ice driving atmosphere' and 'atmosphere driving ice'.

Lead-lag regressions were performed using monthly averaged sea ice indices for December, January and February and monthly mean SLP and SAT data from November through March. A lag of -1 month corresponds to the regression between November SLP/SAT with December sea ice, December SLP/SAT with January sea ice and January SLP/SAT with February sea ice. A lag of +1 corresponds to the regressions between January SLP/SAT with December sea ice, February SLP/SAT with January sea ice and March SLP/SAT with February sea ice. The regressions were performed after removing the climatological mean for each month and combining (not averaging) the monthly averaged data. Similar results are found when performing the lead-lag regressions on individual months in winter (Supplementary Fig 5 and 6). To consider potential relationships with longer lead/lag times, we also performed lead-lag regressions between sea ice from September through May and winter atmospheric circulation and mid-latitude temperatures (Supplementary Fig 8 and Supplementary Discussion 3).

Code availability. Code used to create the figures is available on request from the corresponding author.

Data availability. Model output is available on reasonable request from the corresponding author. ERA-Interim reanalysis data was obtained from the ECMWF data server (https://www.ecmwf.int/en/forecasts/datasets/reanalysis-datasets/era-interim)

References

48. Cavalieri, D. J., Parkinson, C. L., Gloersen, P. & Zwally, H. J. Sea Ice Concentrations from Nimbus-7 SMMR and DMSP SSM/I-SSMIS Passive Microwave Data, Version 1. (1996). doi:http://dx.doi.org/10.5067/8GQ8LZQVL0VL

Figures

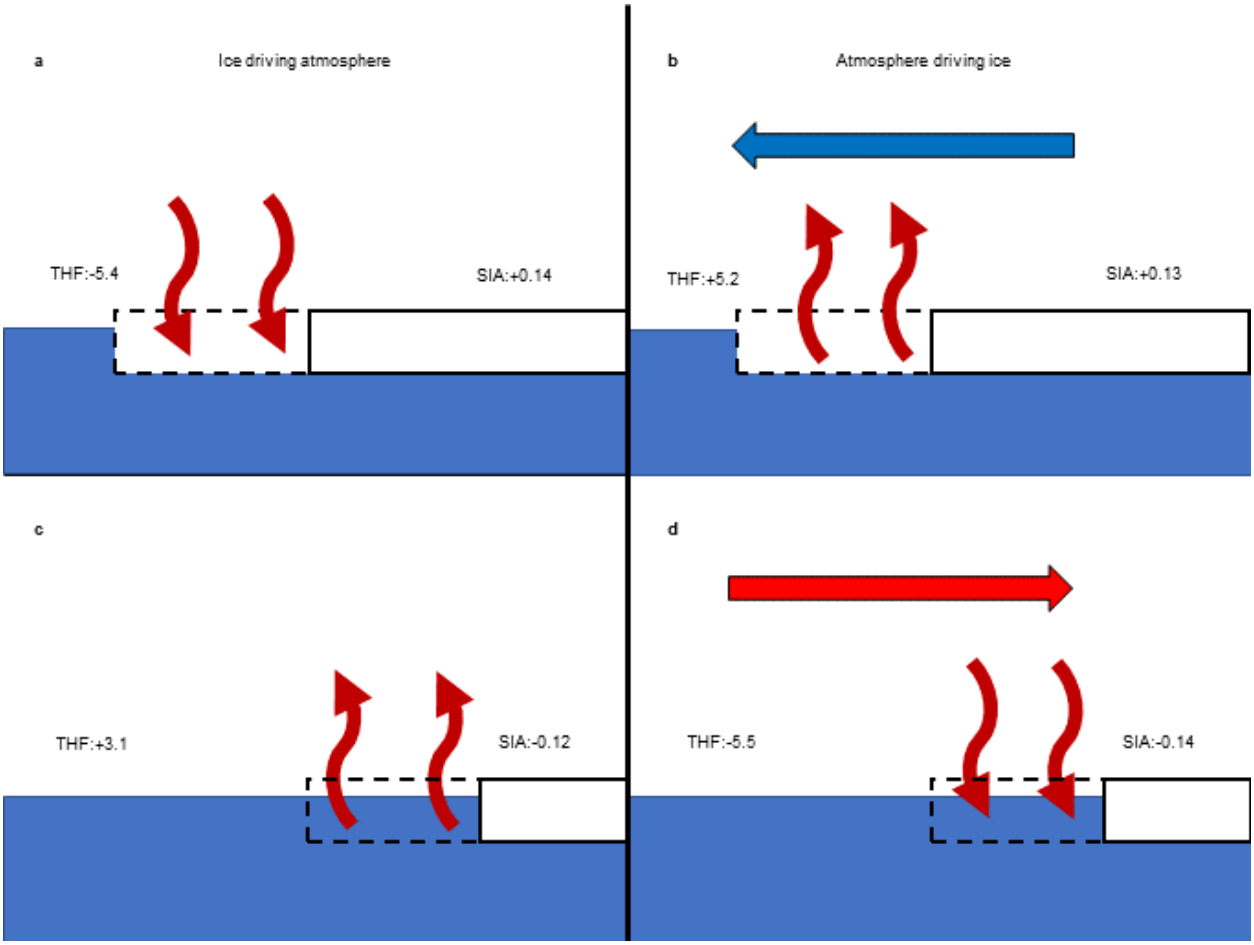

Figure 1: Schematic representation of sea ice driving and being driven by the atmosphere. An illustration of sea ice and THF during winters when sea ice is driving the atmosphere (**a**, **c**) and when the atmosphere is driving the sea ice (**b**, **d**). White rectangles represent sea ice, with the dotted outline indicating the anomalous high or low ice cover. Curved arrows represent the surface THF anomaly and horizontal arrows represent warm (red) and cold (blue) air advection. Composite values for the THF (W m^{-2}) and SIA (10^6 km^2) anomalies averaged over the Chukchi-Bering Sea (165° E -155° W, 55° N-70° N) region for ERA-Interim during winter (December-February) are shown.

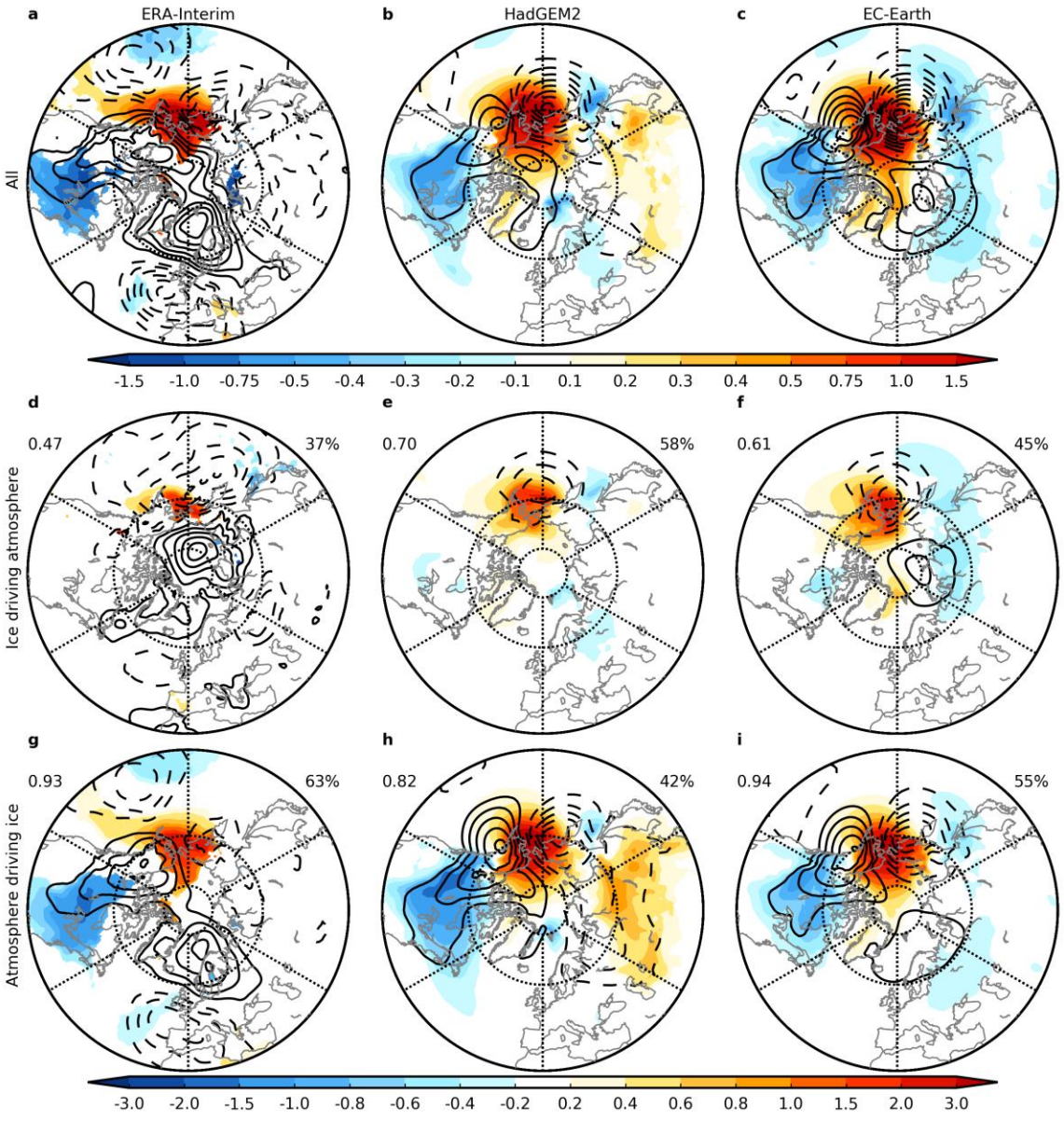

488

489 **Figure 2: Temperature and circulation links with Chukchi-Bering sea ice. a-c** Winter SLP
490 (contours; 0.25 hPa contour intervals) and SAT (coloured shading; °C) regressed on the
491 standardised CBS sea ice index for ERA-Interim (**a**), HadGEM2 (**b**), and EC-Earth (**c**). The sign
492 is reversed so that the maps represent the field associated with a one standard deviation reduction
493 in sea ice area. Coloured shading is only shown where the SAT regression is statistically
494 significant at the 95% confidence level. **d-f** As in **a-c** but only for winters when sea ice is driving

the atmosphere. All contour and shading intervals are double the magnitude of those in **a-c** (0.5 hPa intervals for SLP). Numbers on the top left of the panels indicate the pattern correlation of the SLP fields from 30°-90°N with the corresponding field in panels **a-c**. The percentage of winters when sea ice is driving the atmosphere is indicated on the top right. **g-i** As in **d-f** but only for winters where the atmosphere is driving the sea ice.

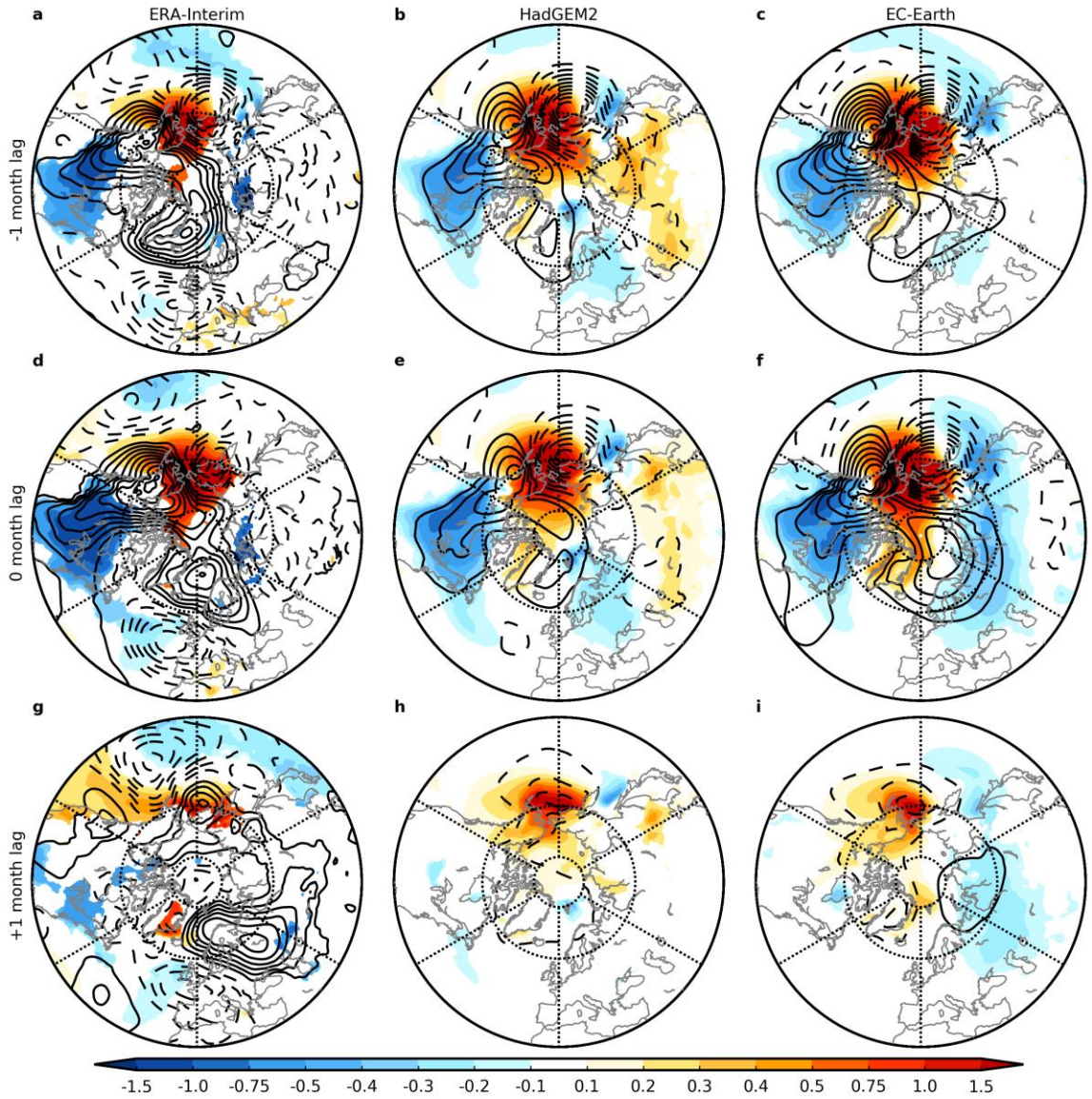

Figure 3: Temperature and circulation lead-lag regressions with Chukchi-Bering sea ice.

SLP (contours; 0.25 hPa contour levels) and SAT (coloured shading; °C) regressed on the CBS sea ice index at -1 month (**a-c**), 0 month (**d-f**) and +1 month (**g-h**) lag in ERA-Interim (**a**, **d**, **g**), HadGEM2 (**b**, **e**, **h**) and EC-Earth (**c**, **f**, **i**). Negative lag indicates the SLP and SAT lead the sea ice. Coloured shading is only shown where the SAT regression is statistically significant at the 95% confidence level.

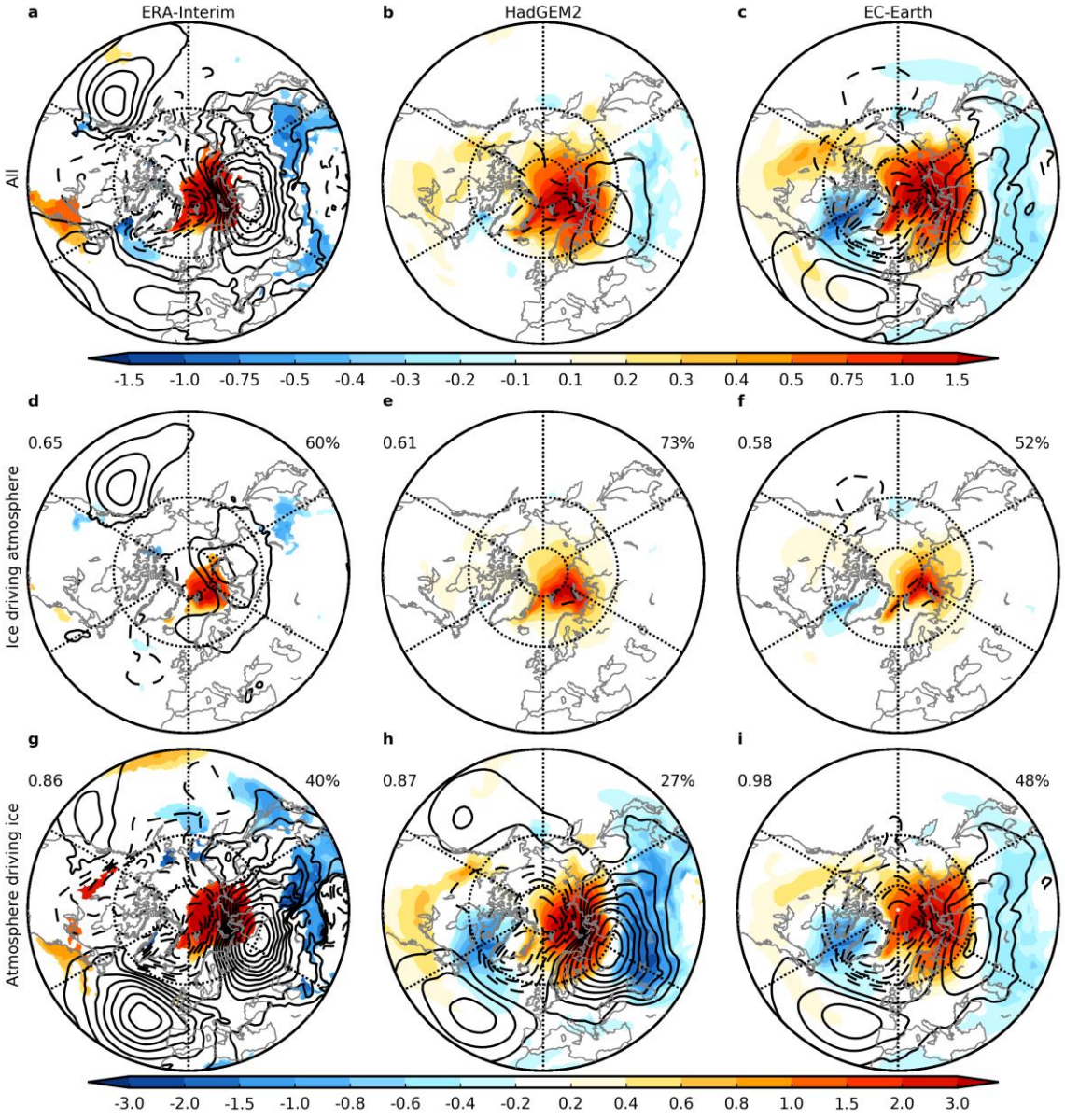

Figure 4: Temperature and circulation links with Barents-Kara sea ice. Winter SLP

(contours; 0.25 hPa contour intervals) and SAT (coloured shading; °C) regressed on the standardised BKS sea ice index for ERA-Interim (**a**), HadGEM2 (**b**), and EC-Earth (**c**). The sign is reversed so that the maps represent the field associated with a one standard deviation reduction in sea ice area. Coloured shading is only shown where the SAT regression is statistically significant at the 95% confidence level. **d-f** As in **a-c** but only for winters when sea ice is driving the atmosphere. All contour and shading intervals are double the magnitude of those in **a-c** (0.5 hPa intervals for SLP). Numbers on the top left of the panels indicate the pattern correlation of the SLP fields from 30°-90°N with the corresponding field in panels **a-c**. The percentage of winters when sea ice is driving the atmosphere is indicated on the top right. **g-i** As in **d-f** but only for winters where the atmosphere is driving the sea ice.

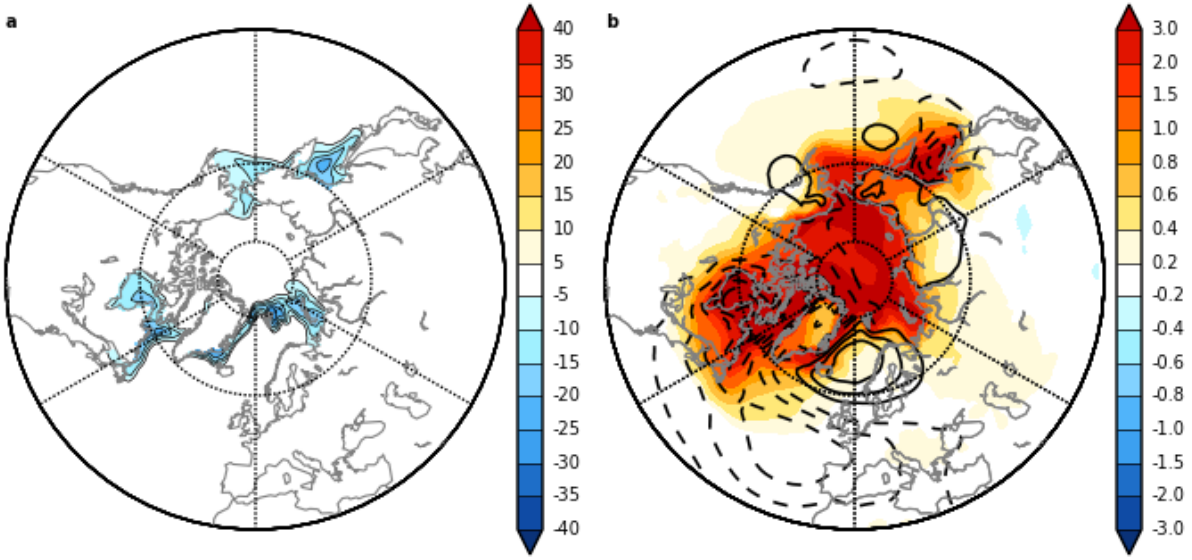

Figure 5: Temperature and circulation response to projected sea-ice loss. a Winter sea ice concentration (%) difference between future and present-day ensembles. **b** As, **a** but for winter SLP (contours; 0.25 hPa contour intervals) and SAT (coloured shading; °C). Coloured shading is only shown where the difference is statistically significant at the 95% confidence level.